

Modulation Doping via a Two-Dimensional Atomic Crystalline Acceptor

Yiping Wang,[□] Jesse Balgley,[□] Eli Gerber, Mason Gray, Narendra Kumar, Xiaobo Lu, Jia-Qiang Yan, Arash Fereidouni, Rabindra Basnet, Seok Joon Yun, Dhavala Suri, Hikari Kitadai, Takashi Taniguchi, Kenji Watanabe, Xi Ling, Jagadeesh Moodera, Young Hee Lee, Hugh O. H. Churchill, Jin Hu, Li Yang, Eun-Ah Kim, David G. Mandrus, Erik A. Henriksen,^{*} and Kenneth S. Burch^{*}

Cite This: *Nano Lett.* 2020, 20, 8446–8452

Read Online

ACCESS |

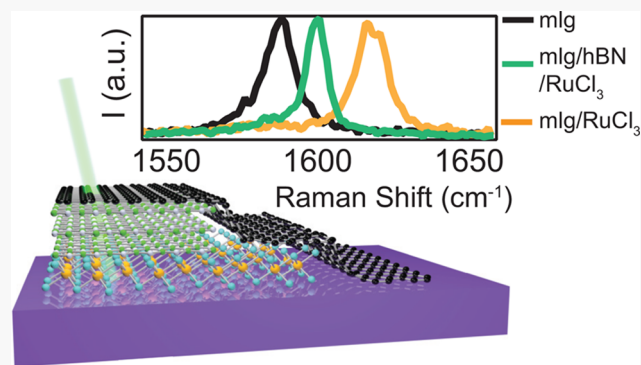
Metrics & More

Article Recommendations

Supporting Information

ABSTRACT: Two-dimensional nanoelectronics, plasmonics, and emergent phases require clean and local charge control, calling for layered, crystalline acceptors or donors. Our Raman, photovoltage, and electrical conductance measurements combined with *ab initio* calculations establish the large work function and narrow bands of α -RuCl₃ enable modulation doping of exfoliated single and bilayer graphene, chemical vapor deposition grown graphene and WSe₂, and molecular beam epitaxy grown EuS. We further demonstrate proof of principle photovoltage devices, control via twist angle, and charge transfer through hexagonal boron nitride. Short-ranged lateral doping (≤ 65 nm) and high homogeneity are achieved in proximate materials with a single layer of α -RuCl₃. This leads to the best-reported monolayer graphene mobilities (4900 cm²/(V s)) at these high hole densities (3×10^{13} cm⁻²) and yields larger charge transfer to bilayer graphene (6×10^{13} cm⁻²).

KEYWORDS: Modulation Doping, 2D Atomic Crystals, Raman, Chemical Vapor Deposition, Molecular Beam Epitaxy, Quantum Oscillations, RuCl₃



Modulation doping in crystalline films¹ produced extreme carrier mobilities for fast/high power electronics,² efficient optoelectronics,^{3–5} qubits,⁶ the fractional quantum Hall effect,⁷ and topological superconductivity.⁸ However, two-dimensional (2d) van der Waals materials lack crystalline dopants for permanent, large, uniform, and local control of charge densities. Previous attempts utilized ionic liquid and polymer electrolyte gating,^{9–16} atomic/molecular intercalation, functionalization, and adsorption.^{17–21} Densities exceeding 10^{14} cm⁻² were achieved in graphene,^{10,13,17,18,20} though at significant cost to sample quality. Furthermore, these chemical approaches cannot be applied to air sensitive materials nor specific layers of the heterostructure. Here, we show these limitations are circumvented with an insulating two-dimensional material that acts as a crystalline acceptor.

We focus on α -ruthenium(III) chloride (α -RuCl₃), a van der Waals, narrow-band Mott insulator with a deep work function of 6.1 eV (Figure 1),²² far greater than the typical work functions of layered materials (~ 4.5 eV). In α -RuCl₃ the onsite Coulomb repulsion (U) and strong spin-orbit coupling (λ_{SOC}) produce strongly narrowed valence and conduction bands that are just 1 eV apart with the Fermi level close to the conduction band edge.^{22,23} Taken together, these properties

imply α -RuCl₃ will accept a large density of electrons. This electronic structure also makes α -RuCl₃ a good insulator^{24,25} and thus is unlikely to interfere with electrical measurements. Further isolation is possible by using a hexagonal boron nitride (hBN) spacer, through which α -RuCl₃ still draws charge. Additionally, this unique electronic structure produces complex magnetic interactions in α -RuCl₃,^{26,27} placing it close to a Kitaev spin liquid phase. Thus, heterostructures could enable novel magnetic states²⁸ and incorporate the topological excitations of α -RuCl₃ into devices. Lastly, for mid-IR plasmonic and optoelectronic applications,²⁹ α -RuCl₃ has minimal optical absorption²³ below the 1 eV gap.

To establish α -RuCl₃ as a crystalline acceptor and bring modulation doping to two-dimensional crystals, we employ spatially resolved Raman spectroscopy. This allows rapid

Received: August 28, 2020
 Revised: November 2, 2020
 Published: November 9, 2020



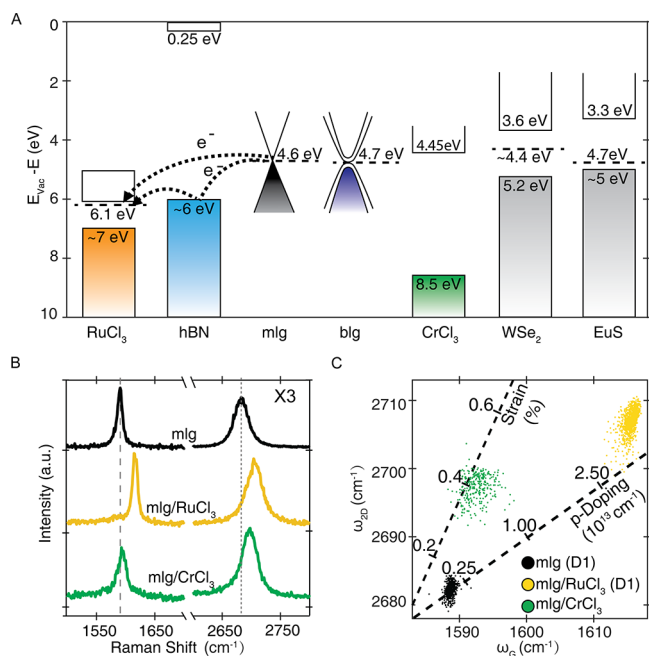


Figure 1. Charge transfer in α -RuCl₃ heterostructures. (A) Band alignment schematic; the work function difference between α -RuCl₃ and other compounds yields charge transfer. (B) Representative Raman spectra for mlg (black trace), mlg/RuCl₃ (yellow trace), and mlg/CrCl₃ (green trace) samples. (C) Correlation between the graphene G and 2D Raman mode for different mlg-based heterostructures, result of only strain or doping indicated with dashed lines.

probing of the induced charge, strain, homogeneity, lateral, and vertical extent of the charge transfer in a variety of α -RuCl₃ heterostructures without fabrication. Our results provide the first unambiguous evidence that even a single layer of α -RuCl₃ is able to strongly charge the target layer even when hBN is between them, including higher doping in bilayer graphene. A variety of proof of principle experiments further point to its utility: creation of a p–p' homojunction for 2D optical sensors and electronics, and charge transfer to chemical vapor deposition-grown (CVD) graphene and WSe₂, as well as molecular beam epitaxy-grown EuS (see SI). In the latter case, the effect on EuS delivered a four-orders-of-magnitude reduction of the measured resistance and an induced hole density of $6.5 \times 10^{13} \text{ cm}^{-2}$ predicted by *ab initio* “mismatched interface theory” (MINT).³⁰ Our combined Raman, transport, and MINT results also point to the ability to tune the charge transfer via twist angle with minimal induced strain, crucial for achieving clean modulation doping with short lateral extent ($\leq 65 \text{ nm}$). This rather small length scale is consistent with theoretical calculations for the formation of p–n junctions in graphene due to mismatched work functions with metal contacts³¹ as well as recent near-field IR experiments.³² The short-range also requires careful optimization to minimize inhomogeneous charge transfer, which we find can be screened for using Raman spectroscopy, leading to clean devices with a single, highly doped conducting channel and the highest mobilities ($4900 \text{ cm}^2/(\text{V s})$) of graphene charged to a similar level.

Recently electronic transport experiments^{24,33} and first-principles calculations^{30,34} also suggested α -RuCl₃ can dope monolayer graphene (mlg) to hole densities of a few 10^{13} cm^{-2} . However, the two experiments also showed Dirac points

close to zero gate voltage. Furthermore, the Hall and quantum oscillation data imply multiple carrier densities or a splitting of the Dirac cone. As we show through careful Raman studies, these features resulted from regions where the two materials do not touch. Indeed, since transport averages over the whole device it will include contributions from both the nearly charge neutral and strongly hole-doped regimes. Creating uniformly doped samples is crucial for eventual device functionality and, according to electronic structure calculations, will strongly effect the electronic properties of the combined system. Beyond disorder, the lateral and vertical extent of the charge transfer, dependence on layer number and relative rotation, ability to charge dope materials beyond mlg, and prototypical devices remain unexplored.

We begin with device (D1), a single monolayer graphene sheet laid across both mono- and bilayer α -RuCl₃, all supported by a SiO₂/Si substrate. This and the other structures measured in this work represent a new class of devices, incorporating α -RuCl₃- or hBN-supported graphene that either lack contacts or have etched contacts at the graphene edge.³⁵ This ensures that the interface between graphene and α -RuCl₃ is not affected by the presence of metallic leads. The room-temperature Raman spectra is shown in Figure 1b for D1 of the pure mlg and mlg/RuCl₃ regions. In the former, we observe G and 2D Raman peaks whose positions $(\omega_G^0, \omega_{2D}^0) = (1581.6 \pm 0.2 \text{ cm}^{-1}, 2676.9 \pm 0.7 \text{ cm}^{-1})$ lie within the range of accepted values for intrinsic graphene with small amounts of local strain and doping from the SiO₂ substrate.^{36–38} In clear contrast, in device regions containing graphene in contact with α -RuCl₃, the G and 2D peaks are both significantly blue-shifted by 30 and 22 cm^{-1} , respectively, indicating sizable charge transfer.

The doping and strain corresponding to the G and 2D peak shifts are determined following a well-established procedure^{37,38} (see SI). In Figure 1c, we plot the established calibrations for pure strain and doping along with the distributions of peak shifts for the pure mlg and mlg/RuCl₃ regions in D1, taken from a spatially resolved Raman map (Figure 2a). The observed peak shifts in mlg/RuCl₃ indicate an induced average carrier density of $\sim 3 \times 10^{13} \text{ cm}^{-2}$, similar to previous reports^{24,33} and predictions.^{30,34} The charge density variations in each device are smaller than the differences between the average values. As discussed below, we associate this with the (uncontrolled) relative twist angle between the graphene and α -RuCl₃. To determine the strain, we assumed it was uniaxial since (i) MINT³⁰ calculations indicate it is dominant, and (ii) this provides better agreement with experiment compared to a biaxial strain model (see SI). No correlation is found between doping and strain with the latter being quite small ($< 0.2\%$).

To determine whether this charge transfer capability is unique to α -RuCl₃ or is generic to all layered halides, we investigate devices incorporating CrCl₃, a magnetic semiconductor with a similar lattice structure to α -RuCl₃. Our density functional theory (DFT) calculations show the conduction band of CrCl₃ is quite close to the Dirac point of graphene (Figure 1a), suggesting it cannot drive a large charge transfer. As expected, the measured Raman spectra (Figure 1b) together with a scatter plot of the peak positions (Figure 1c) from a SiO₂/CrCl₃/mlg/hBN stack reveal shifts of the 2D peak alone, while the G peak remains essentially unchanged. Thus, CrCl₃ primarily produces a strain in the adjacent graphene layer, confirming that charge transfer is not a generic feature of layered halides.

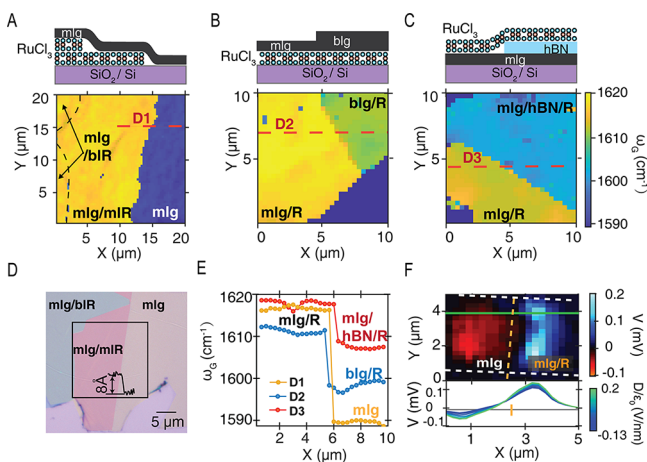


Figure 2. Optical characterization of α -RuCl₃ heterostructures. (A–C) Raman maps of the graphene G peak frequency for different α -RuCl₃ heterostructures with schematics of each heterostructure above their respective maps. (D) False-color optical micrograph of D1, mR is monolayer RuCl₃, bR is bilayer RuCl₃, and R means RuCl₃. Atomic force microscope of monolayer α -RuCl₃ step height (inset). The black square marks the area scanned in (A). (E) Horizontal linecuts of the G peak frequency across the lines indicated in (A–C), revealing the sharp doping change. (F) (Top) Scanning photovoltage map of mlg/ α -RuCl₃ heterostructure acquired at room temperature with a 532 nm laser. mlg is between the white dashed lines, while right of the orange dashed line is covered by α -RuCl₃. (Bottom) Gate voltage dependence of the photovoltage along the green linecut in the scanned photovoltage map, consistent with a p–p' lateral junction.

Next we turn to the thickness dependence of the charge transfer between α -RuCl₃ and graphene layers. First we studied the spatially resolved map of the Raman G peak frequency for device D1 shown in Figure 2a, since this mode has the strongest dependence on the carrier density in mlg. Surprisingly, there is no noticeable change in the G peak frequency of graphene when the laser spot crosses from monolayer α -RuCl₃ to bilayer α -RuCl₃, indicating a single monolayer is sufficient to induce the large hole density.

The same is not true for graphene, where we find that bilayer is more heavily doped than mlg. Specifically, we measured a heterostructure device (D2) having contiguous mono- and bilayer graphene, each partially covering the same flake of α -RuCl₃ (spectra in the SI). We compare the G-peak frequency of the bilayer graphene (blg)/RuCl₃ and mlg/RuCl₃ regions in a map (Figure 2b) and the G/2D distributions in (Figure 4a). Both show the G and 2D peak shifts are smaller in blg/RuCl₃ than in mlg/RuCl₃. However, the density of states is larger in blg, and thus the G peak shift for the same carrier density will be less as it depends on the Fermi level. We find the resulting average carrier density in blg ($6 \times 10^{13} \text{ cm}^{-2}$) is higher than in mlg ($3 \times 10^{13} \text{ cm}^{-2}$). In tandem, we perform self-consistent DFT calculations (details in the SI) for blg/ α -RuCl₃ implemented for AA- and AB-stacked blg. In both cases, we find a larger charge transfer from α -RuCl₃ into blg than mlg (Figure 4e).

Inspired by traditional modulation doping that employs an intermediate insulating layer to separate donors/acceptors from the charged layer, we explored a third device design. Device D3 contains three regions of bare mlg, mlg and α -RuCl₃ in direct contact, as well as mlg and RuCl₃ separated by ≈ 3 nm-thick hBN. As the valence band maximum of hBN is closely aligned with the work function of α -RuCl₃ (Figure 1a),

we anticipate the insulating barrier will reduce—but not entirely eliminate—charge transfer from the mlg. Indeed, the spatially resolved G peak map of D3 (Figure 2c), along with the distribution of 2D and G peak positions (Figure 4a), are consistent with the hBN spacer lowering the induced hole density in mlg to $0.6 \times 10^{13} \text{ cm}^{-2}$. Our DFT calculations of mlg/hBN/RuCl₃ heterostructures suggest this doping is tunable via an inverse relation between the charge transfer and the intermediate hBN thickness (Figure 4c).

The G peak maps of devices D1, D2, and D3 all indicate the lateral charge transfer is short, changing abruptly across the α -RuCl₃ boundary. This is illustrated via the linecuts in Figure 3e, which reveal the doping transition is shorter than the 0.3

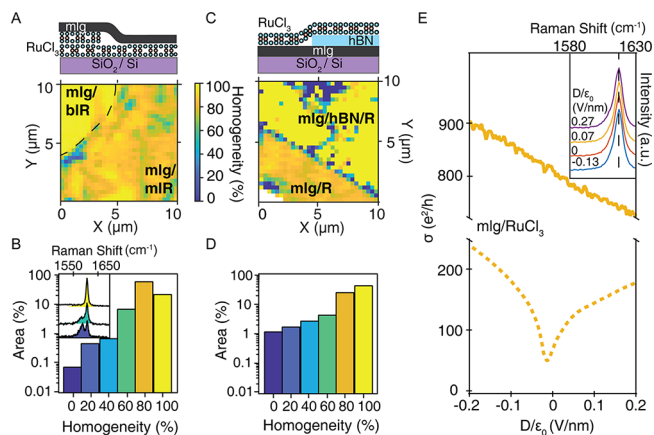


Figure 3. Homogeneity of charge transfer. (A,C) Spatially resolved homogeneity maps for D1 and D3, respectively, with stacking schematics depicted above. (B,D) Histograms of the homogeneity values for each map. (B, inset) Three representative Raman spectra from D1 with varying weights of shifted and unshifted peaks, showing the different homogeneity. (E) Comparison of conductivity versus displacement field D (line scans in Figure 3f) for a RuCl₃/mlg/SiO₂ device with surface contacts between the mlg and α -RuCl₃ (dashed) and a fully encapsulated, edge-contacted hBN/mlg/RuCl₃ device (solid) device. Inset, D -dependence of mlg/RuCl₃ Raman G peak.

μm scanning resolution. The potential utility of this sharp doping profile is demonstrated in room temperature photovoltage measurements shown in Figure 2f for device D4, a graphene channel partially covered with α -RuCl₃. The photovoltage map shows a clear photoresponse at the boundary of the RuCl₃ region, indicating the presence of a p–p' junction leading to a photovoltaic effect. The width of the response is consistent with the spot size of our laser ($\sim 1 \mu\text{m}$) suggesting a sharp doping profile. We ruled out photothermal effects³⁹ by testing both the polarization dependence (data in SI) and the minimal effect of a displacement field D (line scans in Figure 3f). The response seen in graphene not covered by α -RuCl₃ is likely due to inhomogeneous local doping. Indeed, the photovoltage from the uncovered region is suppressed by D , whereas the α -RuCl₃ covered region response is insensitive to D . As such, these results show the potential of α -RuCl₃ in creating homo-junctions of different carrier densities for optoelectronic devices.

Similarly crucial is the homogeneity of the induced charge. Given the short lateral extent, regions where the α -RuCl₃ is not in good contact with graphene could have little to no induced charge, yielding a Raman spectra with both shifted and

unshifted peaks, as shown by the spectra at three different locations of device D1 (inset of Figure 3b). A combination of shifted and unshifted G peaks indicates the presence of both fully doped and charge neutral regions, which likely occurred in previously reported devices. We confirmed this by applying a gate voltage, which moved the center of the unshifted peaks, but not the shifted G peaks as they come from regions with large carrier density (see SI). The relative size of each region within the laser spot is correlated to the spectral weight of the shifted and unshifted peaks with some spectra (yellow shaded trace in Figure 3b inset) revealing no neutral regions. Whether unshifted peaks are present or not, the shifted peaks always appear at the same energy. This is consistent with extremely short-ranged lateral charge transfer, leading to undoped puddles within doped regions with nearly constant induced density. Note that if the chemical potential in α -RuCl₃ were spatially inhomogeneous, we would expect a corresponding distribution of doping in graphene that is not seen in the G peak shifts.

To quantify the uniformity, we define homogeneity to be 100% when only a shifted G peak is present, whereas 0% homogeneous regions exhibit shifted and unshifted peaks with equal spectral weight. We then quantify the device homogeneity as $(2 \times I_{\text{norm}}) - 1$, where I_{norm} is the intensity of the shifted G peak normalized by the sum of intensities of both peaks. The map of sample D1's homogeneity, shown in Figure 3a, reveals a submicron spatial variation. We find some regions with 95% homogeneity, indicative of neutral regions ≤ 65 nm in radius, given our 300 nm resolution (Figure 2e) (details in SI). The homogeneity improves for graphene in contact with bilayer versus monolayer α -RuCl₃ due to better mitigation of the surface roughness of the underlying SiO₂ substrate. Further consistency with our picture that the interface quality is crucial to uniform doping is provided by device D3 (Figure 3c). Here, regions with atomically flat hBN showed improved homogeneity and also revealed in histograms of the homogeneity values for D1 and D3 (see Figure 2b,d). These results imply that Raman spectroscopy can be used to prescreen samples, enabling the deterministic fabrication of clean and homogeneous devices.

These observations resolve outstanding issues in mlg/ α -RuCl₃ devices. Specifically, the appearance of a Dirac point near zero gate voltage in otherwise extremely conductive and highly hole-doped graphene (Figure 3e). The Raman maps for these devices exhibit lesser homogeneity (Figures 2a and 3a) due to numerous neutral regions (unshifted G peak). In contrast, Raman maps in our new devices with smoother interfaces reveal improved homogeneity measured by the absence of neutral regions (Figures 2c and 3c). Meanwhile, the conductivity minimum is lacking in similar devices, as seen in the solid yellow transport trace shown in Figure 3e. Here the Shubnikov–de Haas oscillations show a single population of holes with no additional charge carrier populations (see SI). Transport in device D5 in Figure 3e yields the largest mobility, 4900 cm²/(V s) for single band transport in graphene at correspondingly large densities (3×10^{13} cm⁻²). Competing doping methods, in particular solid electrolyte gating, produce higher densities but result in significant disorder and lower mobilities (see SI Table 1). Preliminary measurements suggest that increasing the distance between the α -RuCl₃ and graphene yields improved sample mobility at the expense of induced charge in the graphene, analogous to conventional modulation

doping in two-dimensional electron gases.¹ Further studies are required and will be the subject of future work.

Lastly, we explain the range of charge transfer in α -RuCl₃ heterostructures via the relative twist angle. Our devices and previous reports indicate a large variation in hole densities over $2\text{--}4 \times 10^{13}$ cm⁻²,^{24,33} far greater than the spread within a single device ($\delta p \approx 1\text{--}5 \times 10^{12}$ cm⁻²) (Figure 4a and SI).

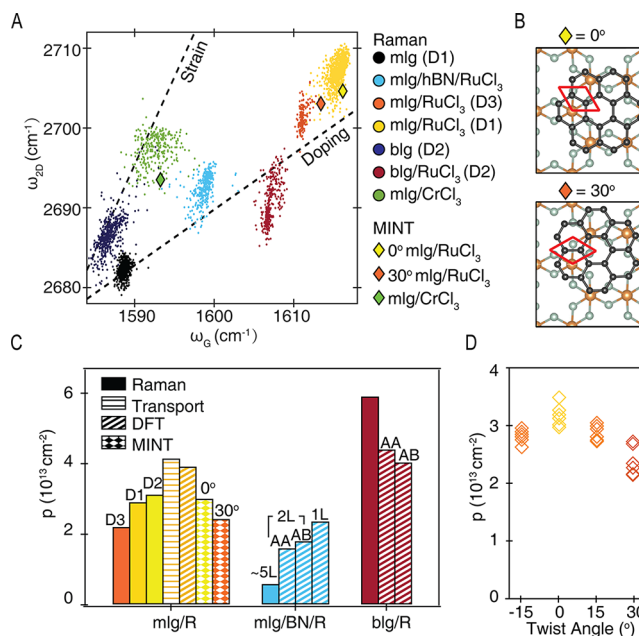


Figure 4. Summary of charge transfer from α -RuCl₃. (A) Correlation between the graphene G and 2D Raman mode for all samples discussed in the text (dots), as well as converted MINT results (diamonds) for different twist angles. (B) Representative MINT supercell alignments for 0° (top) and 30° (bottom) mlg/RuCl₃ twist angles. (C) Doping levels calculated from Raman spectroscopy (filled bars), transport (horizontally striped bars), DFT (diagonally striped bars), and MINT (diamond-checked bars). (D) MINT-calculated mlg doping levels for six graphene supercell positions at different relative twist angles.

Rotating the layers relative to one another changes the overlap between the Ru d and p orbitals, impacting the charge transfer. To this end, Figure 4d shows MINT results for charge transfer at specific angles of the graphene relative to α -RuCl₃ (details in SI). The largest (smallest) charge transfer occurs at an angle of 0° (30°). The calculated carrier densities and strains for these two angles, converted to G and 2D peak frequencies, are plotted in Figure 4a as orange and yellow diamonds, respectively, in close correspondence to the results for devices D1 and D3. The MINT results for a range of angles, shown in Figure 4d, indicate continuous tuning of the charge transfer due to a change in orbital overlap.

In principle, similar effects could emerge from a low work function material acting as a 2D crystalline donor. As such, modulation doping can be introduced into two-dimensional heterostructures with far reaching implications. For example, one can uniformly or locally charge a 2D material by controlling the regions over which it touches a crystalline acceptor or donor. This enables a new regime of two-dimensional plasmonics, improved electrical transparency of contacts by locally doping the contacted layer, and the creation of lateral p–n junctions. Such devices will require expanding

the doping to a wider set of two-dimensional materials, as suggested by Figure 1a, our preliminary molecular beam epitaxy EuS, CVD graphene, and WSe₂ results (SI). Furthermore, the large and local electric fields in α -RuCl₃ will break inversion symmetry. As such, they should enable new nonlinear responses in two-dimensional materials and tune the spin–orbit coupling. Thus, when combined with magnetic two-dimensional atomic crystals, α -RuCl₃ could provide new spintronic devices and topological phases such as skyrmion lattices and spin liquids. Indeed an important question for future studies is the interplay between the magnetism and charge transfer in α -RuCl₃ heterostructures.

■ ASSOCIATED CONTENT

SI Supporting Information

The Supporting Information is available free of charge at <https://pubs.acs.org/doi/10.1021/acs.nanolett.0c03493>.

Details regarding exfoliation and fabrication of devices, experimental measurement setups, peak fittings, and theoretical calculations (PDF)

■ AUTHOR INFORMATION

Corresponding Authors

Erik A. Henriksen – Department of Physics and Institute for Materials Science and Engineering, Washington University in St. Louis, St. Louis, Missouri 63130, United States; orcid.org/0000-0002-4978-2440; Email: henriksen@wustl.edu

Kenneth S. Burch – Department of Physics, Boston College, Chestnut Hill, Massachusetts 02467, United States; orcid.org/0000-0002-7541-0245; Email: ks.burch@bc.edu

Authors

Yiping Wang – Department of Physics, Boston College, Chestnut Hill, Massachusetts 02467, United States

Jesse Balgley – Department of Physics, Washington University in St. Louis, St. Louis, Missouri 63130, United States

Eli Gerber – School of Applied and Engineering Physics, Cornell University, Ithaca, New York 14853, United States

Mason Gray – Department of Physics, Boston College, Chestnut Hill, Massachusetts 02467, United States; orcid.org/0000-0002-2778-9166

Narendra Kumar – Department of Physics, Boston College, Chestnut Hill, Massachusetts 02467, United States

Xiaobo Lu – Department of Physics, Washington University in St. Louis, St. Louis, Missouri 63130, United States

Jia-Qiang Yan – Materials Science and Technology Division, Oak Ridge National Laboratory, Oak Ridge, Tennessee 37831, United States; Department of Materials Science and Engineering, University of Tennessee, Knoxville, Tennessee, United States

Arash Fereidouni – Department of Physics, University of Arkansas, Fayetteville, Arkansas 72701, United States

Rabindra Basnet – Department of Physics, University of Arkansas, Fayetteville, Arkansas 72701, United States

Seok Joon Yun – Center for Integrated Nanostructure Physics, Sungkyunkwan University, Gyeonggi-do, Korea; orcid.org/0000-0002-8695-7166

Dhaval Suri – Francis Bitter Magnet Laboratory and Plasma Science and Fusion Center, Massachusetts Institute of

Technology, Cambridge, Massachusetts 02139, United States; orcid.org/0000-0003-0085-7648

Hikari Kitadai – Department of Chemistry, Boston University, Boston, Massachusetts 02215, United States

Takashi Taniguchi – National Institute for Materials Science, Tsukuba 305-0044, Japan; orcid.org/0000-0002-1467-3105

Kenji Watanabe – National Institute for Materials Science, Tsukuba 305-0044, Japan; orcid.org/0000-0003-3701-8119

Xi Ling – Department of Chemistry, Boston University, Boston, Massachusetts 02215, United States; orcid.org/0000-0003-3462-9088

Jagadeesh Moodera – Department of Physics, Massachusetts Institute of Technology, Cambridge, Massachusetts 02139, United States

Young Hee Lee – Center for Integrated Nanostructure Physics, Sungkyunkwan University, Gyeonggi-do, Korea; orcid.org/0000-0001-7403-8157

Hugh O. H. Churchill – Department of Physics, University of Arkansas, Fayetteville, Arkansas 72701, United States

Jin Hu – Department of Physics, University of Arkansas, Fayetteville, Arkansas 72701, United States; orcid.org/0000-0003-0080-4239

Li Yang – Department of Physics and Institute for Materials Science and Engineering, Washington University in St. Louis, St. Louis, Missouri 63130, United States; orcid.org/0000-0002-8611-6359

Eun-Ah Kim – Department of Physics, Cornell University, Ithaca, New York 14853, United States

David G. Mandrus – Materials Science and Technology Division, Oak Ridge National Laboratory, Oak Ridge, Tennessee 37831, United States; Department of Materials Science and Engineering, University of Tennessee, Knoxville, Tennessee, United States

Complete contact information is available at: <https://pubs.acs.org/doi/10.1021/acs.nanolett.0c03493>

Author Contributions

□ Y.W. and J.B. contributed equally to this work

Author Contributions

Y.W. and J.B. performed the Raman experiments and analyzed the data with the assistance of K.S.B. J.B. fabricated the devices and performed the transport measurements. M.G. assisted in device fabrication. E.G. and E.A.K. performed the MINT calculations. X. Lu and L.Y. performed the DFT calculations. J.Y. and D.M. provided the α -RuCl₃ crystals. A.F., R.B., H.C., and J.H. built the CrCl₃ heterostructures. S.J.Y. and Y.H.L. provided the WSe₂ films. D.S. and J.M. provided EuS films. H.K. and X.Ling grew the CVD graphene, which was transferred by N.K. T.T. and K.W. provided the hBN crystals. Y.W. and J.B. wrote the manuscript with the help of K.B. and E.A.H. and all coauthors. Y.W., J.B., E.G., E.A.K., E.A.H., and K.S.B. contributed to the discussion. K.S.B. and E.A.H. conceived and supervised the project. The data that support the plots within this paper and other findings of this study are available from the corresponding authors on request.

Notes

The authors declare no competing financial interest.

ACKNOWLEDGMENTS

Y.W. and K.S.B. are grateful for the support of the Office of Naval Research under Award number N00014-20-1-2308. J.B. and E.A.H. acknowledge support under National Science Foundation Grant DMR-1810305 and with L.Y. acknowledge support from the Institute of Materials Science and Engineering at Washington University in St. Louis. X.L. and L.Y. are supported by the National Science Foundation CAREER Grant DMR-1455346 and the Air Force Office of Scientific Research Grant FA9550-17-1-0304. D.G.M. acknowledges support from the Gordon and Betty Moore Foundation's EPIQS Initiative, Grant GBMF9069. Work by M.G. was supported by the National Science Foundation Grant DMR-2003343 and N.K. was supported by the U.S. Department of Energy (DOE), Office of Science, Office of Basic Energy Sciences under award no. DE-SC0018675. E.-A.K. was supported by the National Science Foundation (Platform for the Accelerated Realization, Analysis, and Discovery of Interface Materials (PARADIM)) under Cooperative Agreement No. DMR-1539918, and E.G. was supported by the Cornell Center for Materials Research with funding from the NSF MRSEC program (DMR-1719875). D.S. and J.S.M. were supported by CIQMNSF DMR-1231319, NSF Grant DMR1700137 and ONR Grant N00014-16-1-2657 and ARO grant W911NF1920041. R.B., A.F., H.C., and J.H. were supported by the U.S. Department of Energy, Office of Science, Office of Basic Energy Sciences under award no. DE-SC0019467 for CrCl₃ growth and heterostructure fabrication.

REFERENCES

- (1) Natelson, D. *Nanostructures and nanotechnology*; Cambridge University Press: Cambridge, 2015.
- (2) Gonschorek, M.; Carlin, J.-F.; Feltn, E.; Py, M.; Grandjean, N. High electron mobility lattice-matched Al In N/ Ga N field-effect transistor heterostructures. *Appl. Phys. Lett.* **2006**, *89*, 062106.
- (3) Li, Y.; Qian, F.; Xiang, J.; Lieber, C. M. Nanowire electronic and optoelectronic devices. *Mater. Today* **2006**, *9*, 18–27.
- (4) Ross, J. S.; Klement, P.; Jones, A. M.; Ghimire, N. J.; Yan, J.; Mandrus, D. G.; Taniguchi, T.; Watanabe, K.; Kitamura, K.; Yao, W.; Cobden, D. H.; Xu, X. Electrically tunable excitonic light-emitting diodes based on monolayer WSe₂ p–n junctions. *Nat. Nanotechnol.* **2014**, *9*, 268–272.
- (5) Mak, K. F.; Shan, J. Photonics and optoelectronics of 2D semiconductor transition metal dichalcogenides. *Nat. Photonics* **2016**, *10*, 216–226.
- (6) Eriksson, M.; Coppersmith, S.; Lagally, M. Semiconductor quantum dot qubits. *MRS Bull.* **2013**, *38*, 794.
- (7) Tsui, D. C.; Stormer, H. L.; Gossard, A. C. Two-Dimensional Magnetotransport in the Extreme Quantum Limit. *Phys. Rev. Lett.* **1982**, *48*, 1559–1562.
- (8) Shabani, J.; Kjaergaard, M.; Suominen, H. J.; Kim, Y.; Nichele, F.; Pakrouski, K.; Stankevic, T.; Lutchyn, R. M.; Krogstrup, P.; Feidenhans'l, R.; Kraemer, S.; Nayak, C.; Troyer, M.; Marcus, C. M.; Palmstrom, C. J. Two-dimensional epitaxial superconductor-semiconductor heterostructures: A platform for topological superconducting networks. *Phys. Rev. B: Condens. Matter Mater. Phys.* **2016**, *93*, 155402.
- (9) Pachoud, A.; Jaiswal, M.; Ang, P. K.; Loh, K. P.; Özyilmaz, B. Graphene transport at high carrier densities using a polymer electrolyte gate. *EPL (Europhysics Letters)* **2010**, *92*, 27001.
- (10) Ye, J.; Craciun, M. F.; Koshino, M.; Russo, S.; Inoue, S.; Yuan, H.; Shimotani, H.; Morpurgo, A. F.; Iwasa, Y. Accessing the transport properties of graphene and its multilayers at high carrier density. *Proc. Natl. Acad. Sci. U. S. A.* **2011**, *108*, 13002–13006.
- (11) Das, A.; Pisana, S.; Chakraborty, B.; Piscanec, S.; Saha, S. K.; Waghmare, U. V.; Novoselov, K. S.; Krishnamurthy, H. R.; Geim, A. K.; Ferrari, A. C.; Sood, A. K. Monitoring dopants by Raman scattering in an electrochemically top-gated graphene transistor. *Nat. Nanotechnol.* **2008**, *3*, 210–215.
- (12) Bruna, M.; Ott, A. K.; Ijäs, M.; Yoon, D.; Sassi, U.; Ferrari, A. C. Doping Dependence of the Raman Spectrum of Defected Graphene. *ACS Nano* **2014**, *8*, 7432–7441.
- (13) Efetov, D. K.; Kim, P. Controlling Electron-Phonon Interactions in Graphene at Ultrahigh Carrier Densities. *Phys. Rev. Lett.* **2010**, *105*, 256805.
- (14) Chen, F.; Qing, Q.; Xia, J.; Li, J.; Tao, N. Electrochemical Gate-Controlled Charge Transport in Graphene in Ionic Liquid and Aqueous Solution. *J. Am. Chem. Soc.* **2009**, *131*, 9908–9909.
- (15) Browning, A.; Kumada, N.; Sekine, Y.; Irie, H.; Muraki, K.; Yamamoto, H. Evaluation of disorder introduced by electrolyte gating through transport measurements in graphene. *Appl. Phys. Express* **2016**, *9*, 065102.
- (16) Chen, C.-F.; Park, C.-H.; Boudouris, B. W.; Horng, J.; Geng, B.; Girit, C.; Zettl, A.; Crommie, M. F.; Segalman, R. A.; Louie, S. G.; Wang, F. Controlling inelastic light scattering quantum pathways in graphene. *Nature* **2011**, *471*, 617–620.
- (17) Zhao, W.; Tan, P. H.; Liu, J.; Ferrari, A. C. Intercalation of Few-Layer Graphite Flakes with FeCl₃: Raman Determination of Fermi Level, Layer by Layer Decoupling, and Stability. *J. Am. Chem. Soc.* **2011**, *133*, 5941–5946.
- (18) Grüneis, A.; Attacalite, C.; Rubio, A.; Vyalikh, D. V.; Molodtsov, S. L.; Fink, J.; Follath, R.; Eberhardt, W.; Büchner, B.; Pichler, T. Angle-resolved photoemission study of the graphite intercalation compound KC₈: A key to graphene. *Phys. Rev. B: Condens. Matter Mater. Phys.* **2009**, *80*, 075431.
- (19) Elias, J. A.; Henriksen, E. A. Unexpected Hole Doping of Graphene by Osmium Adatoms. *Ann. Phys.* **2020**, *532*, 1900294.
- (20) McChesney, J. L.; Bostwick, A.; Ohta, T.; Seyller, T.; Horn, K.; González, J.; Rotenberg, E. Extended van Hove Singularity and Superconducting Instability in Doped Graphene. *Phys. Rev. Lett.* **2010**, *104*, 136803.
- (21) Zhang, X.; Hsu, A.; Wang, H.; Song, Y.; Kong, J.; Dresselhaus, M. S.; Palacios, T. Impact of Chlorine Functionalization on High-Mobility Chemical Vapor Deposition Grown Graphene. *ACS Nano* **2013**, *7*, 7262–7270.
- (22) Koitzsch, A.; Habenicht, C.; Müller, E.; Knupfer, M.; Büchner, B.; Kandpal, H. C.; van den Brink, J.; Nowak, D.; Isaeva, A.; Doert, T. J_{eff} Description of the Honeycomb Mott Insulator α -RuCl₃. *Phys. Rev. Lett.* **2016**, *117*, 126403.
- (23) Sandilands, L. J.; Sohn, C. H.; Park, H. J.; Kim, S. Y.; Kim, K. W.; Sears, J. A.; Kim, Y.-J.; Noh, T. W. Optical probe of Heisenberg-Kitaev magnetism in α -RuCl₃. *Phys. Rev. B: Condens. Matter Mater. Phys.* **2016**, *94*, 195156.
- (24) Zhou, B.; Balgley, J.; Lampen-Kelley, P.; Yan, J.-Q.; Mandrus, D. G.; Henriksen, E. A. Evidence for charge transfer and proximate magnetism in graphene- α -RuCl₃ heterostructures. *Phys. Rev. B: Condens. Matter Mater. Phys.* **2019**, *100*, 165426.
- (25) Mashhadi, S.; Weber, D.; Schoop, L. M.; Schulz, A.; Lotsch, B. V.; Burghard, M.; Kern, K. Electrical Transport Signature of the Magnetic Fluctuation-Structure Relation in α -RuCl₃ Nanoflakes. *Nano Lett.* **2018**, *18*, 3203–3208.
- (26) Banerjee, A.; Yan, J.; Knolle, J.; Bridges, C. A.; Stone, M. B.; Lumsden, M. D.; Mandrus, D. G.; Tennant, D. A.; Moessner, R.; Nagler, S. E. Neutron scattering in the proximate quantum spin liquid α -RuCl₃. *Science* **2017**, *356*, 1055–1059.
- (27) Wang, Y.; Osterhoudt, G. B.; Tian, Y.; Lampen-Kelley, P.; Banerjee, A.; Goldstein, T.; Yan, J.; Knolle, J.; Ji, H.; Cava, R. J.; Nasu, J.; Motome, Y.; Nagler, S. E.; Mandrus, D.; Burch, K. S. The range of non-Kitaev terms and fractional particles in α -RuCl₃. *npj Quantum Materials* **2020**, *5*, 14.
- (28) Lee, W.-C.; MacDonald, A. H. Modulation doping near Mott-insulator heterojunctions. *Phys. Rev. B: Condens. Matter Mater. Phys.* **2006**, *74*, 075106.

(29) Lee, I.-H.; Yoo, D.; Avouris, P.; Low, T.; Oh, S.-H. Graphene acoustic plasmon resonator for ultrasensitive infrared spectroscopy. *Nat. Nanotechnol.* **2019**, *14*, 313–319.

(30) Gerber, E.; Yao, Y.; Arias, T. A.; Kim, E.-A. Ab Initio Mismatched Interface Theory of Graphene on α -RuCl₃: Doping and Magnetism. *Phys. Rev. Lett.* **2020**, *124*, 106804.

(31) Khomyakov, P. A.; Starikov, A. A.; Brocks, G.; Kelly, P. J. Nonlinear screening of charges induced in graphene by metal contacts. *Phys. Rev. B: Condens. Matter Mater. Phys.* **2010**, *82*, 115437.

(32) Rizzo, D. J. et al. Graphene/ α -RuCl₃: An Emergent 2D Plasmonic Interface. 2007, <https://arxiv.org/abs/2007.07147>.

(33) Mashhadi, S.; Kim, Y.; Kim, J.; Weber, D.; Taniguchi, T.; Watanabe, K.; Park, N.; Lotsch, B.; Smet, J. H.; Burghard, M.; Kern, K. Spin-Split Band Hybridization in Graphene Proximitized with α -RuCl₃ Nanosheets. *Nano Lett.* **2019**, *19*, 4659–4665.

(34) Biswas, S.; Li, Y.; Winter, S. M.; Knolle, J.; Valentí, R. Electronic Properties of α -RuCl₃ in Proximity to Graphene. *Phys. Rev. Lett.* **2019**, *123*, 237201.

(35) Wang, L.; Meric, I.; Huang, P. Y.; Gao, Q.; Gao, Y.; Tran, H.; Taniguchi, T.; Watanabe, K.; Campos, L. M.; Muller, D. A.; Guo, J.; Kim, P.; Hone, J.; Shepard, K. L.; Dean, C. R. One-Dimensional Electrical Contact to a Two-Dimensional Material. *Science* **2013**, *342*, 614–617.

(36) Das, A.; Chakraborty, B.; Piscanec, S.; Pisana, S.; Sood, A. K.; Ferrari, A. C. Phonon renormalization in doped bilayer graphene. *Phys. Rev. B: Condens. Matter Mater. Phys.* **2009**, *79*, 155417.

(37) Lee, J. E.; Ahn, G.; Shim, J.; Lee, Y. S.; Ryu, S. Optical separation of mechanical strain from charge doping in graphene. *Nat. Commun.* **2012**, *3*, 1024.

(38) Gill, S. T.; Hinnefeld, J. H.; Zhu, S.; Swanson, W. J.; Li, T.; Mason, N. Mechanical Control of Graphene on Engineered Pyramidal Strain Arrays. *ACS Nano* **2015**, *9*, 5799–5806.

(39) Gabor, N. M.; Song, J. C. W.; Ma, Q.; Nair, N. L.; Taychatanapat, T.; Watanabe, K.; Taniguchi, T.; Levitov, L. S.; Jarillo-Herrero, P. Hot Carrier-Assisted Intrinsic Photoresponse in Graphene. *Science* **2011**, *334*, 648.